Talanta 217 (2020) 121056

Contents lists available at ScienceDirect

Talanta

journal homepage: www.elsevier.com/locate/talanta

Poly-adenine regulated DNA density on AuNPs to construct efficient DNA walker for microRNA-21 detection

Dan Li[a], Zewei Luo[b], Huifang An[a], Enlai Yang[a], Mengfan Wu[a], Zhijun Huang[b], Yixiang Duan[a,*]

[a] Research Center of Analytical Instrumentation, Key Laboratory of Bio-resource and Eco-environment, Ministry of Education, College of Life Science, Sichuan University, Chengdu, 610065, Sichuan, PR China

[b] Research Center of Analytical Instrumentation, Key Laboratory of Synthetic and Natural Functional Molecule Chemistry of Ministry of Education, College of Chemistry & Materials Science, Northwest University, Xi'an, 710069, Shanxi, PR China

ARTICLE INFO

Keywords:
Poly-adenine
Gold nanoparticles
Density regulation
DNA walker
MicroRNA-21

ABSTRACT

DNA-modified gold nanoparticles (AuNPs) are useful nanomaterials for detecting multiple molecules. However, their performance is greatly dependent on the density of probe DNA on the surface of AuNPs. Here, we used Poly-adenine (PolyA) to regulate the surface density of probe DNA to achieve a highly efficient DNA walking biosensor system to detection miRNA-21. The movement track of the biosensor system consists of PolyA-DNA probe was connected to AuNPs, and exonuclease III (Exo III) acted as a motor driving the walker movement to achieve signal amplification. By optimizing the length of PolyA, the surface density of probe DNA was changed, thereby affecting the target binding and enzymatic processing of the bound probes, which ultimately enhanced the sensitivity and reduced timeliness of the DNA walker. Furthermore, the designed PolyA-DNA probe exhibits an outstanding sensitivity, due to the effect of density regulation, which is 7.9 times and 11.1 times lower than those of the SH-DNA and the free-DNA, respectively. In addition, the hairpin structure of DNA probe locates fluorophore at a zone adjacent to AuNPs surface, which reduces the background signal by 1.1 times compared with traditional straight probe. In this work, the biosensor system shows a high selectivity towards miRNA-21. Moreover, the biosensor system has been demonstrated to be potentially useful for the miRNA-21 detection in human serum with the recoveries of 93.2%–110.0% and has high repeatability. Considering these advantages, this PolyA-regulated DNA walking biosensor system has great potential as a routine tool for miRNA detection and has wide applications in the field of biomedical analysis.

1. Introduction

MicroRNAs (miRNAs) are a class of small (~22 nucleotides), low abundance, single-stranded, non-protein-coding RNAs which regulate post-transcriptional gene expression, cell proliferation and apoptosis [1]. In recent years, researchers have reported that the level of miRNAs expression is closely associated with the occurrence and development of different cancers and other pathological conditions [2,3]. Therefore, the detection of specific miRNAs is of great significance for further understanding the functions of miRNAs and clinical diagnosis.

In the past two decades, a mass of miRNAs analysis methods, such as northern blotting, DNA microarrays and quantitative RT-PCR (qRT-PCR) have been developed [4–7]. However, due to the low abundance of miRNA, those methods have encountered respective challenges in practical analysis, such as low sensitivity, time-consuming and complicated. In order to overcome those defects, new strategies such as fluorescence [8,9], colorimetry [10], electrochemistry [11,12] and DNA walker [13,14] have been explored to improve the performance of miRNAs detection system. Among them, DNA walker was considered to be an efficient method for detecting miRNAs [15,16]. DNA walker is one kind of DNA nanodevice, exhibits a powerful ability to actuate walking chains move along their tracks from starting point to destination, which combines with strand hybridization, enzymatic reaction and environmental stimuli to achieve signal amplification. However, DNA walking devices also met serious challenges in three key performances: difficult trajectory control, shot movement distance and low reaction rates [17]. In order to overcome these challenges and build high performance walking devices, many strategies [18–20] have been developed, the most important being dimensional expansion [21].

Accumulating evidence has demonstrated that DNA walker nanodevices powered by enzymes or strand displacement can move along precisely designed one-dimensional (1D) footpath [22,23] or two-

* Corresponding author.
E-mail address: yduan@scu.edu.cn (Y. Duan).

https://doi.org/10.1016/j.talanta.2020.121056
Received 29 November 2019; Received in revised form 13 April 2020; Accepted 16 April 2020
Available online 20 April 2020
0039-9140/

dimensional (2D) DNA scaffold [24] in terms of dimensionality. The walking path of the 1D footpath is relatively short and the walking chain is difficult to restart after the movement stopped accidently, all of which limit the signal amplification and sensitivity of the constructed biosensor [18,25]. The 2D DNA scaffold shows a DNA motor loaded at one end of the track moves autonomously and has a constant average speed moving along the full length of the track [26,27]. However, owing to long-range transport and hard-operation, this track and motor are difficult to accurate control and design in biosensing [27]. Due to the 1D, 2D limitations described above, the three-dimensional (3D) [21] track has caught the attention of researchers, which can better improve the sensitivity, speed of reaction and has simpler design and accurate control. For example, Yang et al. [28] have recently reported a DNA walker nanodevice that can walks randomly along a 3D track on microparticle surface, which used the Au–S connection on the surface of AuNPs to successfully achieve a large number of connections and stepwise movement of the DNA walker. However, with the in-depth study of the researchers, it has been found that the performance of DNA-modified AuNP-based biosensors is highly dependent on the density of probe DNA. The method of Au–S connection is difficult to control the total number, distance and conformation of DNA probes, thus reducing the hybridization efficiency of DNA walker and the sensitivity of target detection [29,30]. It was found that at low surface coverages, the adjacent DNA probes are separated by a great distance, causing the flexible DNA probe to lodging on the AuNPs surface, leading to nonspecific DNA–Au binding, which changed the conformation and limited the reaction of them with target. At high surface coverages, more DNA probes are attached to the surface of AuNPs, resulting high steric and electrostatic repulsion between adjacent DNA probes. These repulsive forces make interactions with complementary oligonucleotides difficult, resulting in inefficient hybridization [30,31]. In order to solve these issues, Fan's group [32] constructed a 3D track through the connection between PolyA and AuNPs, which is an ideal strategy for forming 3D track. Previous studies have demonstrated that PolyA binds to the AuNPs surface with a high adsorption affinity and has the same binding effect as Au–S connection [33–35]. And Zuo's group [31] found that the surface density of DNA probe can programmably engineer by changing the PolyA length. By adjusting the length of PolyA, the density of probes can be precisely controlled, resulting in the improvement of hybridization ability [36]. Furthermore, DNA probes can form an upright conformation due to the elimination of nonspecific DNA–Au binding by the coverage of PolyA, promoting the reaction between PolyA-DNA and target. Based on these characteristics, this connection has been widely employed to develop biosensors for the diverse targets, including miRNAs [34,37–39].

In this work, we have demonstrated that AuNPs-based 3D DNA walking system for miRNA-21 detection achieved rapid optimization by regulating the length of PolyA to adjust the surface coverage of the DNA. We first systematically studied the optimization of the distance and conformation between adjacent probes by changing the length of PolyA, thereby greatly improving the combined efficiency and sensitivity of the preparation system. On the other hands, adjusting the length of PolyA can change the salt ion concentration on the surface of AuNPs, thereby affecting the reaction speed of Exo III and changing the reaction kinetics. In compare with biosensors based on Au–S connection, the PolyA-based walking system proposed in this paper is a more sensitive detection ability and higher repeatability for miRNA-21 detection. Later, a DNA hairpin probe was applied, which can reduce the background signal by improving the quenching effect of fluorescence of DNA probe on AuNPs surface. Moreover, the designed PolyA synergistic 3D DNA walker can be a promising method for biomolecule detection in clinical diagnosis and mechanism research.

2. Experimental section

2.1. Materials and methods

Hydrogen tetrachloroaurate (III) trihydrate ($HAuCl_4{\cdot}3H_2O$), sodium citrate trihydrate ($Na_3C_6H_5O_7{\cdot}3H_2O$), 2-mercaptoethanol (2-$C_2H_6OS$) were purchased from Sigma-Aldrich (USA) and all were analytical grade. All reagents were dissolved in ultrapure water (18.25 MΩ cm). Exo III was obtained from New England Biolabs (NEB, U.K.). All oligonucleotides listed in Table S1 were synthesized and purified by Sangon Biotechnology Co., Ltd (Shanghai, China), all of which were kept at 94 °C for 3 min, and slowly cool down to room temperature for at least 2 h before use. To create and maintain an RNase-free environment, all aqueous solutions, tubes and tips used in this work were treated with 0.1% DEPC and autoclaved.

2.2. Preparation of gold nanoparticles (AuNPs)

AuNPs (14.10 ± 0.42 nm) were synthesized through the method of sodium citrate reduction of $HAuCl_4$ as previous reported [40,41]. In brief, 3 ml 1% (v/v) $Na_3C_6H_5O_7{\cdot}3H_2O$ was added into the boiling and rapidly stirred 47 ml solution containing 1 ml of $HAuCl_4{\cdot}3H_2O$ (0.01 g/ml), and when the color is stable in wine red, the mixture was kept boiling and stirring for 30 min, then cooled to room temperature with stirring. The obtained AuNPs were stored at 4 °C for further use. The size and morphology of AuNPs were assessed by transmission electron microscopy (TEM) (Tecnai G2 F20 S-TWIN, FEI, USA) and dynamic light scattering (DLS) (Zetasizer nano ZS90, Malvern, UK). The concentration of AuNPs was obtained by C = A 450/ε 450 [42].

2.3. Preparation of PolyA-DNA-AuNPs (PDAs)

AuNPs were functionalized with PolyA-DNA probe in this experiment. Briefly, the obtained AuNPs were aging with PolyA-DNA in a molar ratio (PolyA-DNA/AuNPs) of 200:1 for 16 h at 25 °C without additional NaCl. Buffer A (0.1 M PBS, 2 M NaCl, pH 7.4) was then slowly added to the mixture for salting at room temperature for 40 h (the final concertation of NaCl was 0.2 M). Subsequently, the mixture was centrifuged at 1, 4000 g for 20 min, and then washed with buffer B (10 mM PBS, 0.2 M NaCl, pH 7.4) for three times to remove excess PolyA-DNA. The obtained PDAs were resuspended in buffer C (10 mM PBS, 0.1 M NaCl, 1 mM $MgCl_2$, pH 7.4).

2.4. Preparation of SH-DNA-AuNPs (SDAs)

Thiol-modified DNA was anchored onto the AuNPs according to this method [43]. Briefly, 10 μL of SH-DNA (100 μM) were treated with TCEP (20 mM) for 1 h to cleave the disulfide bond, then diluted into 400 μL. These activated SH-DNA were incubated with 625 μL AuNPs. Then, the NaCl was slowly added and aged for another 24 h to gain 0.1 M final concertation of NaCl. The functionalized AuNPs was centrifugally washed and redissolved in binding buffer to 540 μL and stored at 4 °C for future use.

2.5. Quantification of PolyA-DNA density on AuNPs surface

The density of PolyA-DNA on AuNPs was quantified via the Beer's law using the 2-mercaptoethanol (MCH) [44], the fluorescence (FAM) labelled PolyA-DNA was used. The MCH with a final concentration of 20 mM was added into the PDAs and incubated at 37 °C overnight with shaking. Then the released PolyA-DNA-FAM was collected by centrifugation and measured the fluorescence intensity at 520 nm (PerkinElmer Lambda LS 55, PerkinElmer, USA). The standard linear calibration curves were measured with different concentrations of PolyA-DNA-FAM as shown in Figure S1. The concentration and amount of PolyA-DNA-FAM was calculated using the standard linear calibration curves.

2.6. Polyacrylamide gel electrophoresis (PAGE)

In the gel electrophoresis assay, a test sample containing 5 μL different reaction products and 1 μL 6 × loading buffer is subjected to 10% polyacrylamide gel. The gel was run at 120 V for 35 min in 1 × TAE buffer, and stained with 4S Red Plus nucleic acid stain for 15 min. Then, the images were obtained by a C300 system (Azure, USA).

2.7. Preparation of human serum samples

Healthy human serum was collected by No. 4 West China Teaching Hospital, Sichuan University (West China Hospital ethical clearance letter number: K2017039). First, healthy human serum was centrifuged through 5, 000 g for 6 min. The middle layer of the serum sample was diluted for 5 times by using buffer D (0.1 M PBS, 0.1 M KCl, pH 7.4). Finally, the diluted serum sample was added into the mixture, and then the fluorescence intensity of the final mixture was measured at 520 nm (λex = 494 nm).

3. Results and discussion

3.1. Principle of the exo III- propelled 3D DNA walker

Design of the Exo III- Propelled 3D DNA Walker based on PolyA, and the working principle of biosensor system is shown in Fig. 1. Our 3D DNA Walker contains three components: 3D PDAs track, Exo III and walking strand (miRNA-21). Firstly, the fluorophore (6- FAM) on PolyA-DNA is quenched by nanosurface energy transfer (NSET) [45,46]. Then, the RNA walking strand is first hybridizes with miRNA-21 capture PolyA-DNA probe on the surface of AuNPs, based on the simple rule of Watson-Click base pairing, the hairpin structure of PolyA-DNA probe is opened to form the DNA/RNA heteroduplexes with blunt terminal, and the Exo III gradually digests the 3′ blunt terminal of DNA by burnt-bridge mechanism [14,47], so that the fluorophore as signal reporter is released and monitored. As the number of PolyA-DNA-miRNA-21 complementary bases decreased, miRNA-21 loses its stability and automatically binds to another stands of PDAs and initiates the next cleavage cycle. Hence, the movement of the 3D DNA walker offers an effective approach to transduce and amplify biorecognition signals. By contrast, in the absence of the miRNA-21, the hairpin structure of PolyA-DNA remains on the surface of AuNPs, leading to the FAM-labelled PolyA-DNA is not digested and recovered fluorescence. In view of the way of signal amplification, this Exo III -propelled, PolyA synergistic DNA walker with high target-triggered hybridization efficiency is enable to detect miRNA-21sensitively.

3.2. Feasibility of 3D DNA walker

To verify the feasibility of the proposed biosensor, the connection between PolyA-DNA and AuNPs was characterized at first. As shown in Fig. 2A, the UV/Vis absorption spectrum (PerkinElmer Lambda 25 UV/VIS, PerkinElmer, USA) of bare AuNPs shows the characteristic peak at 517 nm (black line). After functionalizing with PolyA10-DNA probe, the absorption peak of the PDAs shows a tiny red shift (~3 nm) to 520 nm (red line). As shown in Fig. 2B and C, the size of the prepared bare AuNPs is 14.10 ± 0.42 nm and the functionalized PolyA10-DNA-AuNPs (P_{10}DAs) shows the uniform size at 18.32 ± 0.75 nm as shown in Fig. 2D and E. TEM results also shows that the functionalized P_{10}DAs has better dispersion than bare AuNPs. Meantime, the size of digestion P_{10}DAs shows a decreasing trend as shown in Figure S2. These results strongly demonstrated that the PolyA-DNA probes had been successfully modified on the surface of AuNPs. The fastness of PDAs was verified by PolyT according to the simple rule of Watson-Click base pairing. As shown in Figure S3, the presence of PolyT has no remarkable effect on the fluorescence intensity of the PDAs, demonstrating the fastness of the PDAs.

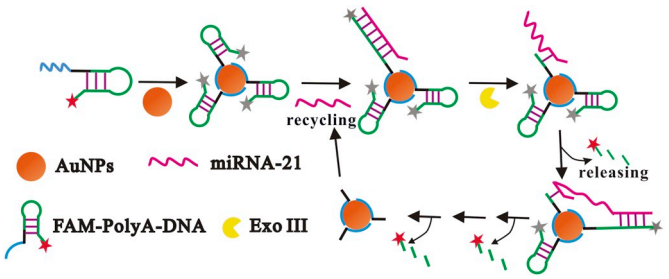

Fig. 1. Illustrates for Exo III- propelled 3D DNA walker based on PolyA moving on the AuNPs surface.

Subsequently, the fluorescence experiment was carried out to verify the feasibility of the 3D DNA walker for miRNA-21 assay. As shown in Fig. 2F, the fluorescence is not well quenched when AuNPs are mixed with PolyA10-DNA without additional NaCl (curve c) compared with a high effective quenching effect on fluorescence mixed with NaCl by salting-aging (curve a). And the spectrum of PolyA10-DNA-FAM with same concentration in solution is shown (curve b). The biosensor cannot achieve signal amplification (curve d) when only miRNA-21-DNA present. In contrast, in the presence of miRNA-21-DNA and Exo III, a relatively strong fluorescence intensity is observed at 520 nm (curve e), which indicating that this biosensor has made effective signal amplification to the targeted RNA.

In addition, the performance of biosensor was also investigated using PAGE assay. As shown in Figure S4, the band of PolyA10-DNA is obviously observed in the absence of additional NaCl (lane 4). When additional NaCl was added into the mixture, no obvious PolyA10-DNA is observed (lane 5), because the PolyA10-DNA is connected to the surface of AuNPs. In the group of miRNA-21-DNA present only (lane 6) in PDAs solution, the band of miRNA-21-DNA is unclear. This is because that some miRNA-21-DNA and PolyA10-DNA formed the double-stranded structures that connected to the surface of AuNPs. However, when miRNA-21-DNA and Exo III are added (lane 7), the band of miRNA-21-DNA is obvious, as the Exo III digested the double-stranded structure and released the miRNA-21-DNA. All the above results strongly prove that the designed biosensor is a rational strategy for detecting miRNA-21.

3.3. Regulation of PolyA-DNA density on the surface of AuNPs

Some previous reports have shown that DNA with different PolyA lengths have different connection density on the surface of AuNPs [48]. In other words, the PolyA length could adjust the final amount of PolyA-DNA loaded on AuNPs, which is vital factor on the sensitivity of target detection. To obtain an optimal performance, PolyA lengths of DNA probe were investigated in this work. The PolyA-DNA-FAM on the surface of AuNPs was released by using MCH, which can break interaction between single-stranded DNA (ss-DNA) and AuNPs [38,49]. As shown in Figure S5, the fluorescence intensity of the PDAs is low (curve b). Meanwhile, the fluorescence is strongly recovered (curve c) by using MCH, which could reach 94.2% of the free DNA probe (curve a). The density of PolyA on AuNPs surface was calculated by normalizing the recovery fluorescence intensity.

In this experiment, DNA probes with PolyA5, PolyA10, PolyA20, PolyA30 and PolyA40 tail were respectively loaded on the AuNPs surface. As shown in Fig. 3B, as the length of PolyA increases, the DNA probes attached to AuNP reduces gradually. However, the number of adenines connected to per AuNP are approached (Fig. 3C), which is consistent with the previous reports [32,34]. In the meantime, those results confirmed that the amount of PolyA-DNA loaded on AuNPs surface decreases as the length of PolyA increases as shown in Fig. 3A, indicating that the distance between adjacent PolyA-DNA probes

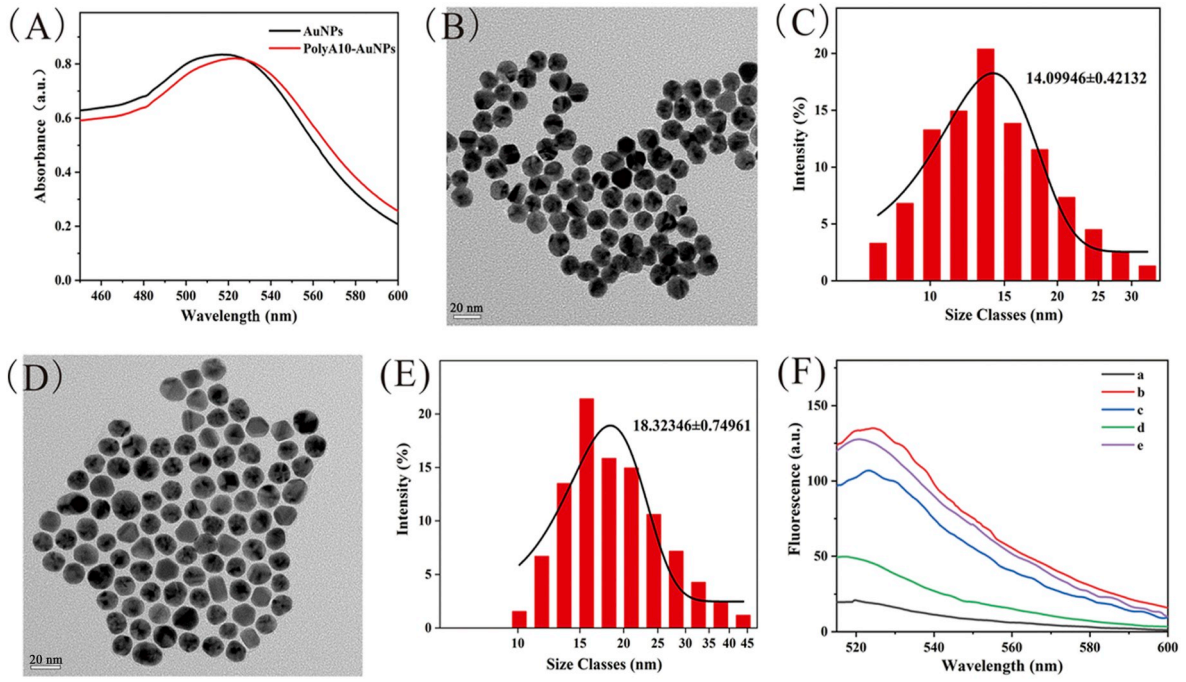

Fig. 2. Characterizations of the connection between PolyA-DNA and AuNPs and feasibility of the walking system. (A) UV/Vis spectra of AuNPs before (black) and after (red) coating with PolyA10-DNA. (B) The TEM image of the bare AuNPs. The scale bar is 20 nm. (C) The DLS result of the bare AuNPs. (D) The TEM image of the functionalized AuNPs. The scale bar is 20 nm. (E) The DLS result of the functionalized AuNPs. (F) The fluorescence measurement of verifying the feasibility of 3D DNA nanomachine. Reaction condition: curve a: 100 μL PolyA10-DNA-AuNPs (P_{10}DAs); curve b: 1.8 μM PolyA10-DNA; curve c: 100 μL AuNPs and 1.8 μM PolyA10-DNA without additional NaCl; curve d: 1.2 nM miRNA-21-DNA, 100 μL P_{10}DAs; curve e: 1.2 nM miRNA-21-DNA, 100 μL P_{10}DAs, 0.06 U/μL Exo III. (For interpretation of the references to color in this figure legend, the reader is referred to the Web version of this article.)

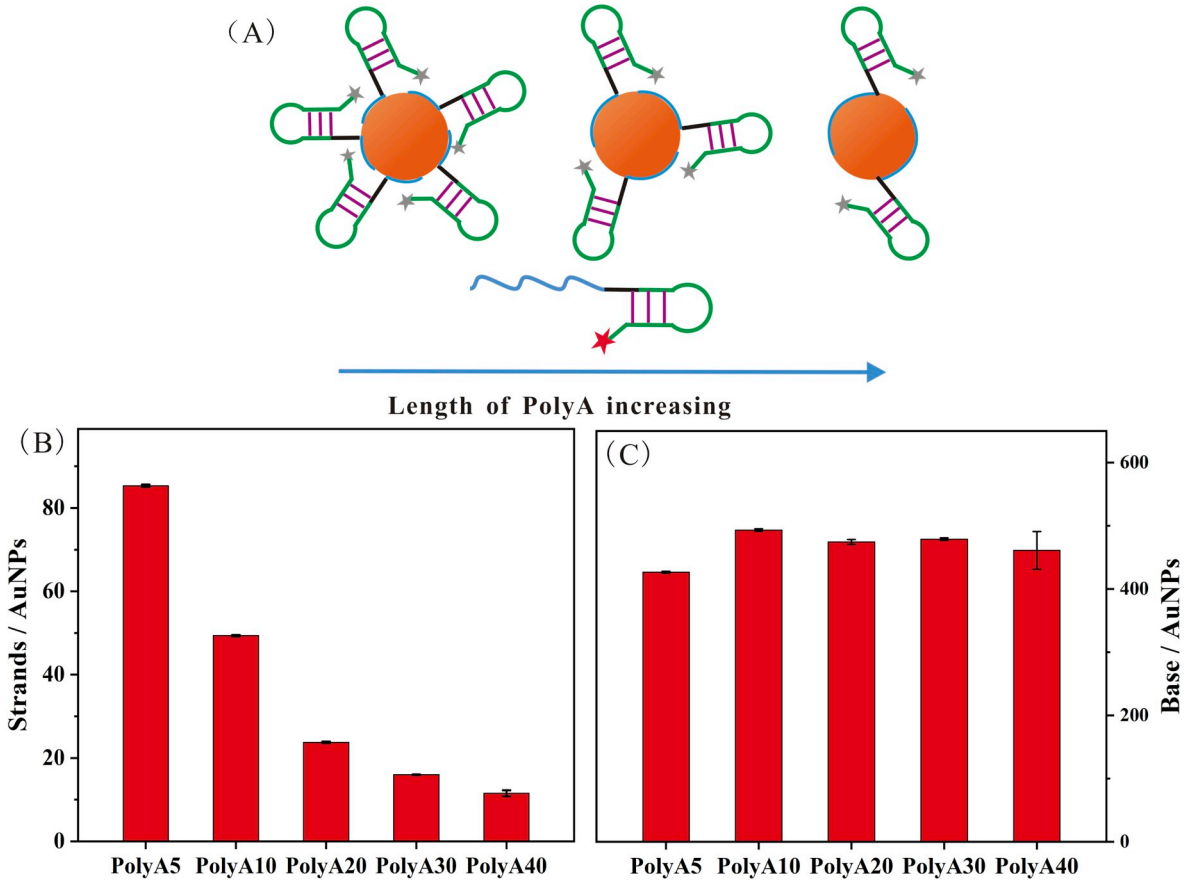

Fig. 3. Density changes with PolyA length. (A) Schematic diagram of spatial control on AuNPs by varying the PolyA length. (B) Surface density of assembled PolyA-DNA (Strands/AuNPs). (C) Surface amount in terms of adenine bases (Base/AuNPs). Each experiment was conducted for three times.

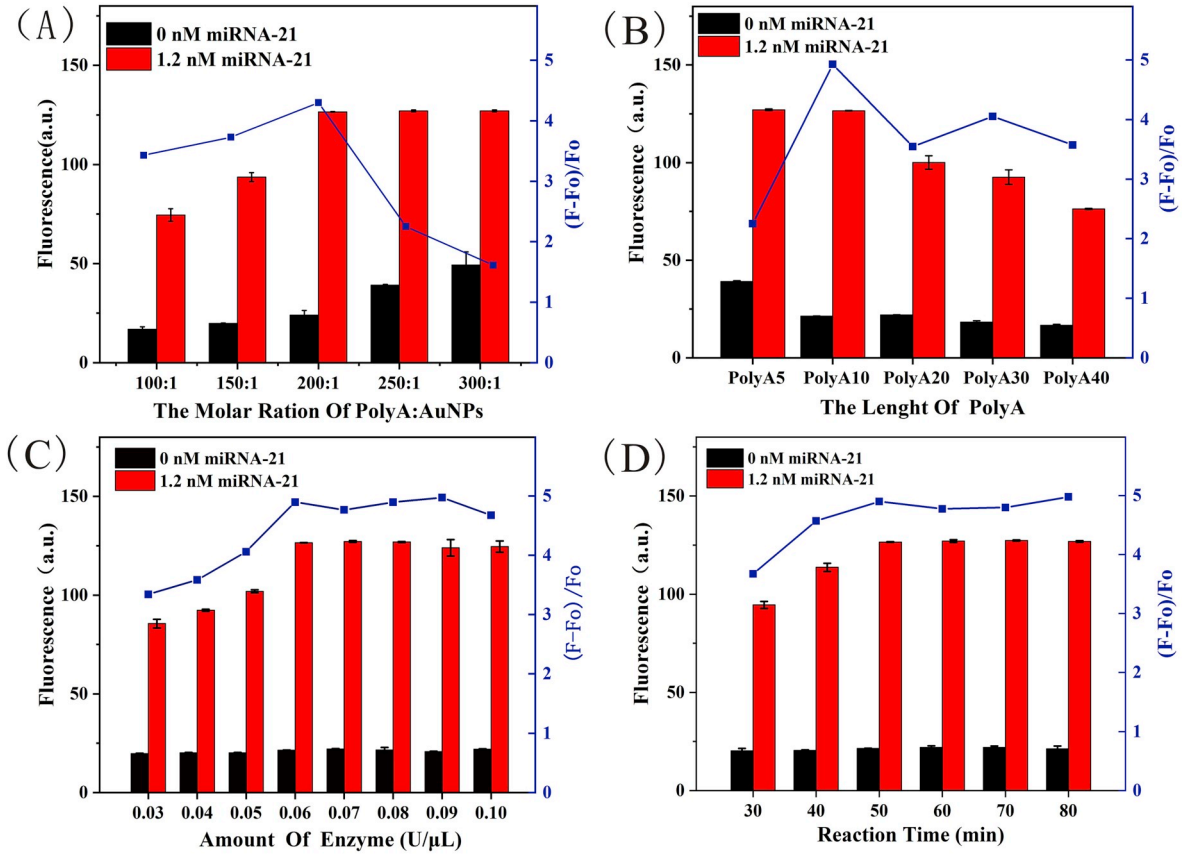

Fig. 4. Optimization of key parameters. (A) Fluorescence analysis of PolyA-DNA/AuNPs at different molar ratios, including 100:1, 150:1, 200:1, 250:1 and 300:1. (B) The change of fluorescence intensity of different length of PolyA including PolyA5, PolyA10, PolyA20, PolyA30, PolyA40-DNA. (C) Effect of the amount of Exo III. Reaction conditions: 100 μL P_{10}DAs, 0/1.2 nM miRNA-21 and different amount of Exo III. (D) Effect of reaction time. Reaction conditions: 100 μL P_{10}DAs, 0/1.2 nM miRNA-21 and 0.06 U/μL Exo III using different reaction time.

increases. In addition, this deduction was also proved by gel electrophoresis (Figure S6).

3.4. Optimization of experimental parameters

To acquire the optimal performance for miRNA-21 detection, four key experimental parameters, including the molar ratio of PolyA-DNA/AuNPs, the length of PolyA, the amount of Exo III and reaction time were optimized. Firstly, molar ratios of PolyA-DNA/AuNPs ranging were tested. As shown in Fig. 4A, as the molar ratio increases from 100:1 to 300:1, the background signal increases gradually, since more residual free PolyA-DNA-FAM cannot be quenched by AuNPs. Meanwhile, when 1.2 nM of miRNA-21 is tested, the fluorescence intensity increases gradually from 100:1 to 200:1, and reaches a plateau when the molar ratio further increased. This is probably because PDAs of 200:1 have enough DNA probes to combine with miRNA-21 to generate fluorescence signal. Thus, the further increase of molar ration only improves the background signal. According to the change of (F-Fo)/Fo ratio, the molar ratio of 200:1 was applied in the followed experiments.

Secondly, the influence of PolyA length on the biosensor performance was further investigated. As shown in Fig. 4B, the background signal decreases gradually as the PolyA length changed from PolyA5 to PolyA40, since the conformation of DNA probe has changed. However, when 1.2 nM of miRNA-21 is tested, the fluorescence signal increases from PolyA5 to PolyA10 and then decreases. Meantime, the increase in fluorescence signal was also calculated as shown in Figure S7, all of which made PolyA10 have the supreme (F-Fo)/Fo ratio and ability of controlling the density to achieve the optimal performance of 3D DNA walker.

Thirdly, the process of signal amplification is closely related to the amount of Exo III, it was also optimized in this work. As shown in Fig. 4C, when the amount of Exo III increases from 0.03 U/μL to 0.06 U/μL, the signals increases obviously, but the signals don't increase significantly when more Exo III are used. Meanwhile, the background signals are nearly constant as the amount of Exo III increased. Hence, 0.06 U/μL Exo III was selected in the following experiments.

Fourthly, in order to achieve timeless and rapid detection, the reaction time was investigated. As shown in Fig. 4D, the relative fluorescence remarkably increases when the reaction time increases from 30 min to 50 min and then remains almost constant from 50 min to 80 min. At the same time, the background signals don't change significantly with time. To achieve the desired results, 50 min was selected as the reaction time in this work.

3.5. Superiority of PolyA synergistic 3D DNA walker biosensor

Based on the above research findings, the change in length of PolyA affects the density and confirmation of DNA probes on the surface of AuNPs, thereby the hybridization efficiency of biosensor was also changed. Therefore, we infer that the density of PolyA-DNA probe is related to the performance of 3D DNA walker. To prove our speculation, the reaction kinetics of different PolyA length were detected by monitoring fluorescence intensity in real-time. As shown in Fig. 5A, firstly, the maximum fluorescence signal of walking system decreases as the length of PolyA increases (from top to bottom), because the number of DNA probes connected to the AuNPs surface is reduced. Secondly, the reaction equilibrium time reduces gradually from 65 to 30 min, when the DNA density was tuned from high to low. However, the

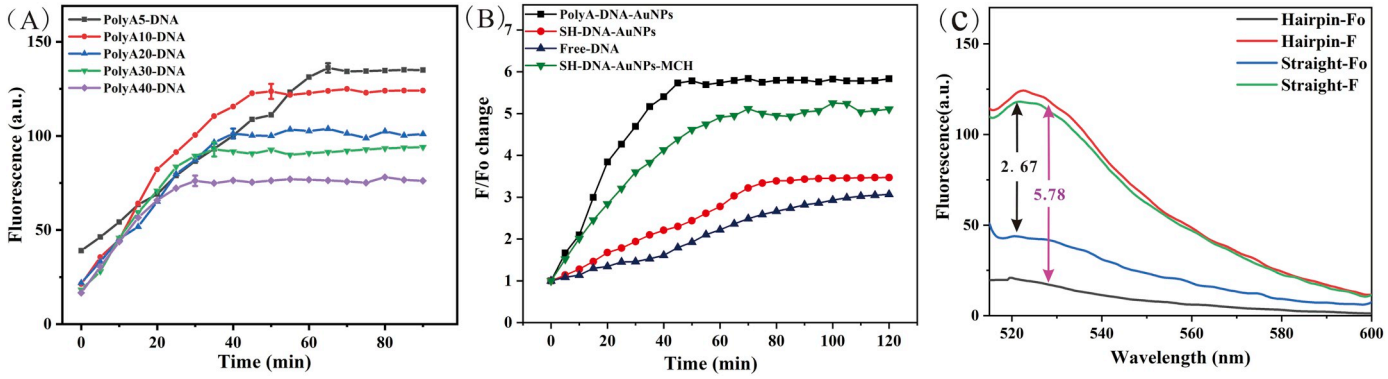

Fig. 5. Superiority of PolyA synergistic walking system. (A) Comparison of time-dependent reaction kinetics curve of different length of PolyA of detecting miRNA-21. Reaction conditions: 100 μL PDAs, 1.2 nM miRNA-21 and 0.06 U/μL Exo III. (B) Comparison of time-dependent fluorescence spectra of different kinds of method of detecting miRNA-21 in response to the same concentration of miRNA-21. Reaction conditions: 100 μL P_{10}DAs/SDAs/SDAs-MCH/1.8 nM Free-DNA, 1.2 nM miRNA-21 and 0.06 U/μL Exo III. (C) Compare the F/Fo ratio between Hairpin-PolyA10-DNA and Straight-PolyA10-DNA. Fo is background signal, F is experimental signal. Reaction conditions: 100 μL hairpin/straight PDAs, 1.2 nM miRNA-21 and 0.06 U/μL Exo III.

reaction speed of Exo III has different changes according to the slope of reaction kinetics curve. These slopes displayed the maximum reaction speed of Exo III is PolyA10-DNA, which indicted that PolyA10-DNA efficiently control the distance of adjacent DNA probes, which is beneficial to the movement and enzymolysis of Exo III. By reaction kinetics experimental result, the best performance of 3D DNA Walker is obtained by PolyA10-DNA.

Next, the reaction kinetics of PDAs using PolyA10, SDAs [36] and free DNA probe were tested by time-dependent fluorescence analysis. When the three biosensors were mixed with the same concentration of miRNA-21, the changes in fluorescence intensity over time were measured every 5 min. As shown in Fig. 5B, the reaction equilibrium time of PDAs is 2.4 times faster than free DNA, and 1.6 times faster than SDAs, indicating that the reaction speed of PDAs is significantly improved. Meanwhile, as shown in Figure S8, the fluorescence intensity of PDAs in equilibrium is about 7.4 times higher than that of free DNA, and 1.7 times higher than that of SDAs, indicating the highest reaction efficiency of PDAs. In the PDAs system, the van der Waals force [50] between AuNPs and PolyA-DNA probe is reduced because the surface of AuNPs is coated with adenines, which can keep the DNA probe upright on the surface of AuNPs, so that miRNA-21 is easy to move under the digestion of Exo III, resulting in efficient reaction speed and excellent performance of constructed biosensor. On the contrary, the SH-DNA probe causes the inhomogeneity lodging on AuNPs surface [47], which seriously affects the movement of walking chain and result in the reduced of biosensor performance. To validate this, we treated the SH-DNA probe based AuNPs surface with MCH, which can minimize the nonspecific binding between the DNA and AuNPs. After treatment, the reaction kinetics of the SDAs increased, indicating the minimization of nonspecific adsorption can improve the biosensor performance (Fig. 5B, green line). And free DNA has no fixed trajectory, leading to discontinuity in the process of signal amplification, which weakens the enzyme-driven reaction kinetics and makes the constructed biosensor perform poorly. Therefore, it is believed that the method of PolyA connection can significantly improve the biosensor performance by precisely controlling the DNA density and conformation.

At the same time, the effect of the shape of the PolyA-DNA probe on the biosensor was also investigated. As shown in Fig. 5C, the background fluorescence intensity of the hairpin structure probe is 1.1 times lower than that of the traditional straight structure probe. The reason is that the PolyA-DNA probe was designed as a hairpin structure to minimize the distance between the fluorophore and AuNPs, which leads to better quenching effect of fluorescence intensity. When the same concentration of miRNA-21 is added, the fluorescence intensity of the hairpin structure probe increases 5.7 times, while the straight structure probe was only 2.6 times by the calculation of F/Fo ratio. Namely, the hairpin structure probe shows higher biosensor performance than the straight structure so that the hairpin configuration offers a new choice for 3D DNA walker biosensor.

3.6. Performance of PolyA synergistic 3D DNA walker

Under the optimized reaction conditions, the walking system PolyA10-DNA synergistic was further applied to the analysis of miRNA-21. A series of different concentrations of miRNA-21 were tested and the corresponding fluorescence spectra were recorded by fluorescence spectrophotometer. Fig. 6A displays the fluorescence intensity changes of 3D DNA walker biosensor upon the introduction miRNA-21 with different concentrations. Fig. 6B shows the relationship between the miRNA-21 concentration and the fluorescence intensity change at 520 nm, indicating that fluorescence intensity increases remarkably with the addition of miRNA-21 at various concentrations ranging from 0 to 400 nM and then remains nearly constant. The inset in Fig. 6B shows the calibration curve for analyzing the miRNA-21. A good linear correlation (R^2 = 0.998) was observed between the fluorescence intensity and the miRNA-21 concentrations in the range of 20 pM–2.5 nM, and the detection limit was calculated to be 8.9 pM based on a signal to noise ratio (S/N) of 3. Meantime, the fluorescence spectra of SDAs (Figure S9) and free DNA (Figure S10) were measured and calibration curves were given. Through the same calculation method, the detection limit of SDAs is 69.9 pM, which was 7.9 times higher than that of PDAs and the detection limit of free DNA is 98.6 pM, which was 11.1 times higher than that of PDAs, indicating the highest Performance of PDAs for miRNA-21 detection. Compared with other 3D DNA walker biosensors, this sensing platform displayed better or comparable sensitivity toward miRNA-21 (Table S2).

3.7. Selectivity of the 3D DNA walker

In order to evaluate the selectivity of the proposed biosensor, the analytical signals of miRNA-21 were compared with those control groups, including miRNA-141 [51], miRNA-429 and miRNA-200b [52]. As shown in Fig. 7, a great relative fluorescence enhancement is obtained when miRNA-21 is added. However, the enhanced intensity for control groups is about one-sixth of that for the targeted miRNA-21 at the same concentration. Because the weak hybridization between other miRNAs and PolyA-DNA probe, it is so difficult to form double-stranded structure that Exo III is unable to digest the 3′ blunt terminal and then fluorescence signal cannot be released. The results validated the feasibility of our proposed sensor to discriminate miRNA-21 and other miRNAs.

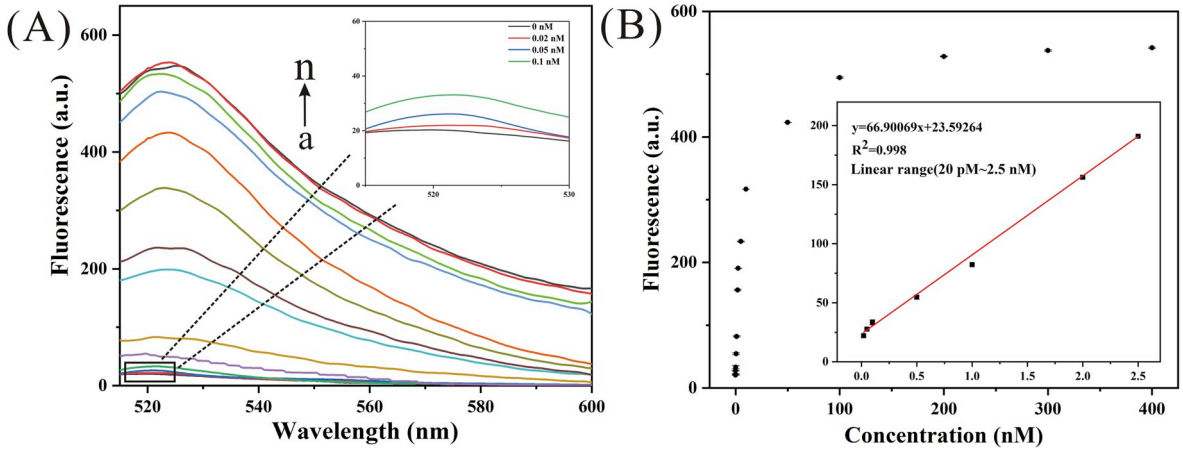

Fig. 6. Performance of the constructed 3D DNA walker biosensor. (A) Fluorescence responses of the present biosensor to different concentrations of miRNA-21. The curves from bottom to top correspond to 0, 0.02, 0.05, 0.1, 0.5, 1, 2.5, 5, 10, 50, 100, 200, 300, 400 nM targeted RNA, respectively. (B) The relationship between the concentration of miRNA-21 and the fluorescence intensity. The inset is the calibration curve.

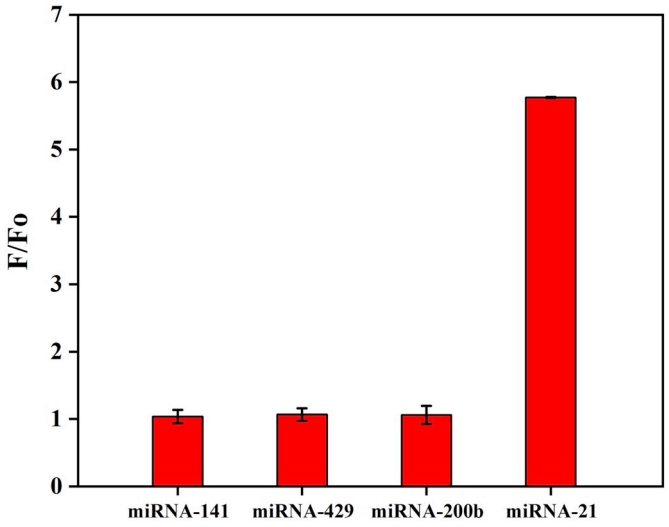

Fig. 7. Fluorescence intensity changes signal/background of the sensing platform for detecting different targets: 1.2 nM miRNA-141, 1.2 nM miRNA-429, 1.2 nM miRNA-200b and 1.2 nM miRNA-21.

3.8. Detection of the miRNA-21 in human serum

It has been reported that miRNA-21 is a stable circulating miRNA in human serum and its levels are associated with cancer [53], so that the analyzing performance of the 3D DNA walker system was also assessed by spiking targets of varying concentrations in human serum. The solution with miRNA-21 was used as a sample for analysis by the proposed sensor and human serum solution as a blank. As demonstrated in Table 1, following the concentration of targeted RNA in the serum varied between 0.05 nM and 1 nM, the spiked recovery is varied within the range of 93.2–110.0% and the relative standard deviation (RSD) varies from 1.2% to 3.4%. According to these results, this biosensor can be used for real samples and has great potential application of cancer detection.

4. Conclusion

In this work, a 3D DNA walking system for miRNA-21 detection by using PolyA regulated density of DNA-Modified AuNPs was constructed. By tuning the length of PolyA, the surface coverage and conformation of adjacent DNA probes were exactly regulated to programmably adjustment the biosensor performance, which is a challenging problem in the biomolecule–nanoparticle research. In addition, the PolyA covers the surface of AuNPs by salting-aging method and the localized DNA probe efficiently avoids the lodging on 3D surface, which is beneficial to the movement and timeliness of DNA walking system. Furthermore, by rational structure design of PolyA-DNA probe, we minimized the distance that deceased the background signal to maintain the biosensor performance. With these advantages, this new strategy can be applied to detect other interested targets. We believe that these novel three-dimensional DNA walkers can provide opportunities for better application of new biomolecule–nanoparticle research. Our proposed has great potential to develop DNA walker devices applied into cancer diagnosis field.

Author contributions

The experiments were designed and performed by Dan Li. Data analysis was performed by Dan Li, Huifang An, Enlai Yang and Mengfan Wu. Manuscript was written by Dan Li, modified by Zewei Luo, Zhijun Huang and Yixiang Duan.

Table 1
Application of the proposed biosensor for targeted RNA detection in human[a] (n = 3).

Sample	Original miRNA-21 (nmol/L)[b]	Target added (nmol/L)	Detected by the Sensor (nmol/L)	Spiked Recovery (%)	RSD (%)
human serum	0.0245	0.050	0.0795	110.0	2.4
		0.500	0.4905	93.2	3.4
		1.000	0.9855	96.1	1.2

[a] The mean concentrations were calculated by the linear curve of the proposed miRNA-21 biosensor.
[b] The dilution factor was 5, because 20 μL of actual human serum was tested in a total reaction volume of 100 μL.

Declaration of competing interest

The authors declare no competing financial interest.

Acknowledgements

This research was gratefully supported by the National Natural Science Foundation of China (No. 21874095). Miaozi Project in Science and Technology Innovation Program of Sichuan Province (No. 2019094). Chengdu Technology Innovation Research and Development Project (No. 2018-YF05-01184-SN). Natural Science Foundation of Shaanxi Province (No. 2020JQ-573). The authors also thank the Analytical & Testing Center of Sichuan University for TEM measurements.

Appendix A. Supplementary data

Supplementary data to this article can be found online at https://doi.org/10.1016/j.talanta.2020.121056.

References

[1] A. Ventura, T. Jacks, MicroRNAs and cancer: short RNAs go a long way, Cell 136 (4) (2009) 586–591.
[2] A. Lujambio, S.W. Lowe, The microcosmos of cancer, Nature 482 (7385) (2012) 347–355.
[3] J. Lu, G. Getz, E.A. Miska, E. Alvarez-Saavedra, J. Lamb, D. Peck, A. Sweet-Cordero, B.L. Ebert, R.H. Mak, A.A. Ferrando, MicroRNA expression profiles classify human cancers, Nature 435 (7043) (2005) 834–838.
[4] W. Li, K. Ruan, MicroRNA detection by microarray, Anal. Bioanal. Chem. 394 (4) (2009) 1117–1124.
[5] J. Li, B. Yao, H. Huang, Z. Wang, C. Sun, Y. Fan, Q. Chang, S. Li, X. Wang, J. Xi, Real-time polymerase chain reaction microRNA detection based on enzymatic stem-loop probes ligation, Anal. Chem. 81 (13) (2009) 5446–5451.
[6] J.M. Thomson, J. Parker, C.M. Perou, S.M. Hammond, A custom microarray platform for analysis of microRNA gene expression, Nat. Methods 1 (1) (2004) 47–53.
[7] S. Sharbati-Tehrani, B. Kutz-Lohroff, R. Bergbauer, J. Scholven, R. Einspanier, miR-Q: a novel quantitative RT-PCR approach for the expression profiling of small RNA molecules such as miRNAs in a complex sample, BMC Mol. Biol. 9 (1) (2008) 34–47.
[8] Q. Xi, D.-M. Zhou, Y.-Y. Kan, J. Ge, Z.-K. Wu, R.-Q. Yu, J.-H. Jiang, Highly sensitive and selective strategy for microRNA detection based on WS2 nanosheet mediated fluorescence quenching and duplex-specific nuclease signal amplification, Anal. Chem. 86 (3) (2014) 1361–1365.
[9] C. Wang, H. Zhang, D. Zeng, W. Sun, H. Zhang, A. Aldalbahi, Y. Wang, L. San, C. Fan, X. Zuo, Elaborately designed diblock nanoprobes for simultaneous multicolor detection of microRNAs, Nanoscale 7 (38) (2015) 15822–15829.
[10] J. Park, J.-S. Yeo, Colorimetric detection of microRNA miR-21 based on nanoplasmonic core–satellite assembly, Chem. Commun. 50 (11) (2014) 1366–1368.
[11] Y. Wen, M. Lin, H. Pei, N. Lu, C. Fan, Electrochemical-based microRNA sensors, Prog. Chem. 24 (9) (2012) 1656–1664.
[12] M. Lin, Y. Wen, L. Li, H. Pei, G. Liu, H. Song, X. Zuo, C. Fan, Q. Huang, Target-responsive, DNA nanostructure-based E-DNA sensor for microRNA analysis, Anal. Chem. 86 (5) (2014) 2285–2288.
[13] P. Yin, H. Yan, X.G. Daniell, A.J. Turberfield, J.H. Reif, A unidirectional DNA walker that moves autonomously along a track, Angew. Chem. Int. Ed. 43 (37) (2004) 4906–4911.
[14] M. Xiao, K. Zou, L. Li, L. Wang, Y. Tian, C. Fan, H. Pei, Stochastic DNA walkers in droplets for super-multiplexed bacterial phenotype detection, Angew. Chem. Int. Ed. 131 (43) (2019) 15594–15600.
[15] L. Wang, R. Deng, J. Li, Target-fueled DNA walker for highly selective miRNA detection, Chem. Sci. 6 (12) (2015) 6777–6782.
[16] Z.-G. Wang, J. Elbaz, I. Willner, DNA machines: bipedal walker and stepper, Nano Lett. 11 (1) (2010) 304–309.
[17] Y. Xing, B. Liu, J. Chao, L. Wang, DNA-based nanoscale walking devices and their applications, RSC Adv. 7 (75) (2017) 47425–47434.
[18] Z. Wu, G.-Q. Liu, X.-L. Yang, J.-H. Jiang, Electrostatic nucleic acid nanoassembly enables hybridization chain reaction in living cells for ultrasensitive mRNA imaging, J. Am. Chem. Soc. 137 (21) (2015) 6829–6836.
[19] S. Bi, S. Yue, S. Zhang, Hybridization chain reaction: a versatile molecular tool for biosensing, bioimaging, and biomedicine, Chem. Soc. Rev. 46 (14) (2017) 4281–4298.
[20] L. He, D. Lu, H. Liang, S. Xie, X. Zhang, Q. Liu, Q. Yuan, W. Tan, mRNA-initiated, three-dimensional DNA amplifier able to function inside living cells, J. Am. Chem. Soc. 140 (1) (2017) 258–263.
[21] N. Li, J. Zheng, C. Li, X. Wang, X. Ji, Z. He, An enzyme-free DNA walker that moves on the surface of functionalized magnetic microparticles and its biosensing analysis, Chem. Commun. 53 (60) (2017) 8486–8488.
[22] D.A. Leigh, U. Lewandowska, B. Lewandowski, M.R. Wilson, Synthetic Molecular Walkers, Molecular Machines and Motors, Springer, 2014, pp. 111–138.
[23] M. Xiao, X. Wang, L. Li, H. Pei, Stochastic RNA walkers for intracellular microrna imaging, Anal. Chem. 91 (17) (2019) 11253–11258.
[24] T.-H. Hsu, S.-L. Nyeo, Diffusion coefficients of two-dimensional viral DNA walks, Phys. Rev. E. 67 (5) (2003) 051911-1-051911-8.
[25] C. Wang, J. Ren, X. Qu, A stimuli responsive DNA walking device, Chem. Commun. 47 (5) (2011) 1428–1430.
[26] S.F. Wickham, M. Endo, Y. Katsuda, K. Hidaka, J. Bath, H. Sugiyama, A.J. Turberfield, Direct observation of stepwise movement of a synthetic molecular transporter, Nat. Nanotechnol. 6 (3) (2011) 166–169.
[27] K. Lund, A.J. Manzo, N. Dabby, N. Michelotti, A. Johnson-Buck, J. Nangreave, S. Taylor, R. Pei, M.N. Stojanovic, N.G. Walter, Molecular robots guided by prescriptive landscapes, Nature 465 (7295) (2010) 206–210.
[28] X. Yang, Y. Tang, S.D. Mason, J. Chen, F. Li, Enzyme-powered three-dimensional DNA nanomachine for DNA walking, payload release, and biosensing, ACS Nano 10 (2) (2016) 2324–2330.
[29] W.J. Parak, T. Pellegrino, C.M. Micheel, D. Gerion, S.C. Williams, A.P. Alivisatos, Conformation of oligonucleotides attached to gold nanocrystals probed by gel electrophoresis, Nano Lett. 3 (1) (2003) 33–36.
[30] P. Liang, J. Canoura, H. Yu, O. Alkhamis, Y. Xiao, Dithiothreitol-regulated coverage of oligonucleotide-modified gold nanoparticles to achieve optimized biosensor performance, ACS Appl. Mater. Interfaces 10 (4) (2018) 4233–4242.
[31] D. Zhu, H. Pei, J. Chao, S. Su, A. Aldalbahi, M. Rahaman, L. Wang, L. Wang, W. Huang, C. Fan, Poly-adenine-based programmable engineering of gold nanoparticles for highly regulated spherical DNAzymes, Nanoscale 7 (44) (2015) 18671–18676.
[32] H. Pei, F. Li, Y. Wan, M. Wei, H. Liu, Y. Su, N. Chen, Q. Huang, C. Fan, Designed diblock oligonucleotide for the synthesis of spatially isolated and highly hybridizable functionalization of DNA–gold nanoparticle nanoconjugates, J. Am. Chem. Soc. 134 (29) (2012) 11876–11879.
[33] S.M. Schreiner, D.F. Shudy, A.L. Hatch, A. Opdahl, L.J. Whitman, D.Y. Petrovykh, Controlled and efficient hybridization achieved with DNA probes immobilized solely through preferential DNA-substrate interactions, Anal. Chem. 82 (7) (2010) 2803–2810.
[34] L. Chen, J. Chao, X. Qu, H. Zhang, D. Zhu, S. Su, A. Aldalbahi, L. Wang, H. Pei, Probing cellular molecules with PolyA-based engineered aptamer nanobeacon, ACS Appl. Mater. Interfaces 9 (9) (2017) 8014–8020.
[35] A. Opdahl, D.Y. Petrovykh, H. Kimura-Suda, M.J. Tarlov, L.J. Whitman, Independent control of grafting density and conformation of single-stranded DNA brushes, P. Natl. Acad. SCI. USA. 104 (1) (2007) 9–14.
[36] K. Yang, H. Wang, N. Ma, M. Zeng, H. Luo, D. He, Programmable target-initiated DNAzyme walker walking along a spatially isolated and highly hybridizable substrate track on a nanoparticle surface, ACS Appl. Mater. Interfaces 10 (51) (2018) 44546–44553.
[37] D. Zhu, J. Chao, H. Pei, X. Zuo, Q. Huang, L. Wang, W. Huang, C. Fan, Coordination-mediated programmable assembly of unmodified oligonucleotides on plasmonic silver nanoparticles, ACS Appl. Mater. Interfaces 7 (20) (2015) 11047–11052.
[38] D. Zhu, P. Song, J. Shen, S. Su, J. Chao, A. Aldalbahi, Z. Zhou, S. Song, C. Fan, X. Zuo, PolyA-mediated DNA assembly on gold nanoparticles for thermodynamically favorable and rapid hybridization analysis, Anal. Chem. 88 (9) (2016) 4949–4954.
[39] G. Yao, H. Pei, J. Li, Y. Zhao, D. Zhu, Y. Zhang, Y. Lin, Q. Huang, C. Fan, Clicking DNA to gold nanoparticles: poly-adenine-mediated formation of monovalent DNA-gold nanoparticle conjugates with nearly quantitative yield, NPG Asia Mater. 7 (1) (2015) 159–166.
[40] G. Frens, Controlled nucleation for the regulation of the particle size in monodisperse gold suspensions, Nat. Phys. Sci. (Lond.) 241 (105) (1973) 20–22.
[41] Z. Huang, J. Chen, Z. Luo, X. Wang, Y. Duan, Label-free and enzyme-free colorimetric detection of Pb2+ based on RNA cleavage and annealing-accelerated hybridization chain reaction, Anal. Chem. 91 (7) (2019) 4806–4813.
[42] W. Haiss, N.T. Thanh, J. Aveyard, D.G. Fernig, Determination of size and concentration of gold nanoparticles from UV− Vis spectra, Anal. Chem. 79 (11) (2007) 4215–4221.
[43] J.I. Cutler, E. Auyeung, C.A. Mirkin, Spherical nucleic acids, J. Am. Chem. Soc. 134 (3) (2012) 1376–1391.
[44] S. Park, K.A. Brown, K. Hamad-Schifferli, Changes in oligonucleotide conformation on nanoparticle surfaces by modification with mercaptohexanol, Nano Lett. 4 (10) (2004) 1925–1929.
[45] T. Jennings, M. Singh, G. Strouse, Fluorescent lifetime quenching near d= 1.5 nm gold nanoparticles: probing NSET validity, J. Am. Chem. Soc. 128 (16) (2006) 5462–5467.
[46] C. Yun, A. Javier, T. Jennings, M. Fisher, S. Hira, S. Peterson, B. Hopkins, N. Reich, G. Strouse, Nanometal surface energy transfer in optical rulers, breaking the FRET barrier, J. Am. Chem. Soc. 127 (9) (2005) 3115–3119.
[47] X. Qu, D. Zhu, G. Yao, S. Su, J. Chao, H. Liu, X. Zuo, L. Wang, J. Shi, L. Wang, An exonuclease III-powered, on-particle stochastic DNA walker, Angew. Chem. Int. Ed. 56 (7) (2017) 1855–1858.
[48] W. Wang, X. Ding, M. He, J. Wang, X. Lou, Kinetic adsorption profile and conformation evolution at the DNA-gold nanoparticle interface probed by dynamic light scattering, Anal. Chem. 86 (20) (2014) 10186–10192.
[49] H. Li, L.J. Rothberg, Label-free colorimetric detection of specific sequences in genomic DNA amplified by the polymerase chain reaction, J. Am. Chem. Soc. 126 (35) (2004) 10958–10961.
[50] K. Liu, H. Li, Y. Wang, X. Gou, Y. Duan, Adsorption and removal of rhodamine B from aqueous solution by tannic acid functionalized graphene, Colloids Surf., A 477 (2015) 35–41.
[51] J. Lu, L. Wu, Y. Hu, S. Wang, Z. Guo, Ultrasensitive Faraday cage-type

electrochemiluminescence assay for femtomolar miRNA-141 via graphene oxide and hybridization chain reaction-assisted cascade amplification, Biosens. Bioelectron. 109 (2018) 13–19.
[52] I. Eisenberg, N. Nahmias, M.N. Persky, C. Greenfield, D. Goldman-Wohl, A. Hurwitz, R. Haimov-Kochman, S. Yagel, T. Imbar, Elevated circulating micro-ribonucleic acid (miRNA)-200b and miRNA-429 levels in anovulatory women, Fertil. Steril. 107 (1) (2017) 269–275.
[53] H. Dong, J. Lei, L. Ding, Y. Wen, H. Ju, X. Zhang, MicroRNA: function, detection, and bioanalysis, Chem. Rev. 113 (8) (2013) 6207–6233.